First results from the ionospheric radio occultations of Saturn by the Cassini spacecraft

Andrew F. Nagy,[1] Arvydas J. Kliore,[2] Essam Marouf,[3] Richard French,[4] Michael Flasar,[5] Nicole J. Rappaport,[2] Aseel Anabtawi,[2] Sami W. Asmar,[2] Douglas Johnston,[2] Elias Barbinis,[2] Gene Goltz,[2] and Don Fleischman[2]

Received 3 November 2005; revised 17 February 2006; accepted 15 March 2006; published 30 June 2006.

[1] The first set of near-equatorial occultations of the Saturn ionosphere was obtained by the Cassini spacecraft between May and September of 2005. The occultations occurred at near-equatorial latitudes, between 10°N and 10°S, at solar zenith angles from about 84° to 96°. The entry observations correspond to dusk conditions and the exit ones to dawn. An initial look at the data indicates that the average peak densities are lower and the peak altitude higher at dawn than at dusk, possibly the result of ionospheric decay during the night hours. There are also significant differences between individual dawn and dusk occultations; the initial thought is that this variation must be connected to changes in the water inflow into the upper atmosphere and/or variations in the particle impact ionization rates.

Citation: Nagy, A. F., et al. (2006), First results from the ionospheric radio occultations of Saturn by the Cassini spacecraft, *J. Geophys. Res.*, *111*, A06310, doi:10.1029/2005JA011519.

1. Introduction

[2] The design of the Cassini spacecraft's tour of the Saturnian system allows multiple radio occultations of Saturn's ionosphere to be carried out. A group of eight near-equatorial occultations was completed during the period 2 May to 5 September 2005. On four of these (orbits, or revs 7, 8, 10 and 12), the near-equatorial path of Cassini behind Saturn allowed probing of the ionosphere on the dusk side during occultation entry and, about three hours later, on the dawn side during occultation exit. On the other four, three exit-only occultations (dawn side: revs 9, 11, and 13) and one entry-only occultation (dusk side: rev 14) were completed, for a total of twelve ionospheric radio occultation observations. A typical ionospheric occultation period is about 10 min. A summary of the observations is presented in Table 1, and Figure 1 shows the associated latitudes and solar zenith angles.

2. Data Acquisition

[3] A simplified diagram of the Cassini radio science system, both on the spacecraft and on the ground, is shown in Figure 2. During the occultation period, Cassini transmits three sinusoidal radio signals of 0.94, 3.6, and 13 cm-wavelength (Ka-, X-, and S-band, respectively). They are coherently generated on board Cassini from a common ultrastable crystal oscillator (USO) which has a typical Allan deviation better than about 2×10^{-13} over 1 to 100 s time intervals. The coherency allows accurate measurement of individual signal frequency as well as differential effects. The longest wavelength, S-band, is particularly sensitive to plasma along the radio path and hence is the primary signal for probing tenuous regions of Saturn's ionosphere. However, regions of large refractivity gradients, such as those near the peak, produce multipath at S-band, and the higher frequencies are more useful there. The differential S/X and X/Ka measurements were used to derive the electron density profiles, as they are sensitive only to dispersive media, i.e., the ionosphere and the interplanetary plasma.

[4] The Cassini signals perturbed by Saturn's ionosphere are received and recorded at the ground stations of the NASA/JPL Deep Space network (DSN). To maximize the observation signal-to-noise ratio (SNR), the 70-m diameter DSN stations were used to receive the X- and S-band signals. The Ka-band receiving capability is presently available only at the smaller 34-m diameter Beam-Waveguide DSN stations. Depending on the particular occultation, either one or two of the three DSN complexes (Goldstone, Madrid, Canberra) were used. Typical free-space SNR achieved is 54, 48, and 42 dB-Hz at X-, Ka-, and S-band, respectively. These levels of SNR are unprecedented in radio occultation investigations, and they are instrumental in producing the very narrow error bars in the electron density profiles.

[5] The DSN Stations are equipped with two types of receivers. The Tracking Receiver is a closed loop system

[1]Department of Atmospheric, Oceanic, and Space Sciences, University of Michigan, Ann Arbor, Michigan, USA.
[2]Jet Propulsion Laboratory, California Institute of Technology, Pasadena, California, USA.
[3]Department of Electrical Engineering, San Jose State University, San Jose, California, USA.
[4]Astronomy Department, Wellesley College, Wellesley, Massachusetts, USA.
[5]NASA Goddard Space Flight Center, Greenbelt, Maryland, USA.

0148-0227/06/2005JA011519

Table 1. A Summary of Cassini Rev 7–14 Saturn Ionosphere Observations

Observation	Date	Latitude, deg	SZA, deg	Dawn /Dusk	Upper Pk		Lower Pk		SEP Angle, deg	Baseline Sigma, cm^{-3}
					n_e, cm^{-3}	Altitude, km	n_e, cm^{-3}	Altitude, km		
S7 Entry	3 May 2005	4.9S	84.4	Dusk	4195	1860	6670	1380	69	18
S7 Exit		9.0S	95.9	Dawn	2220	2420	1011	1160		19
S8 Entry	21 May 2005	3.1S	85.2	Dusk	5697	1940	7937	1540	53	36
S8 Exit		8.3S	95.1	Dawn	937	3020	1265	1580		17
S9 Exit	8 June 2005	7.4S	93.9	Dawn	473	2080	1899	1220	37	19
S10 Entry	26 June 2005	1.6N	87.7	Dusk	6666	1880	2076	1560	22	28
S10 Exit		6.1S	92.3	Dawn	1073	2460	376	1540		35
S11 Exit	15 July 2005	4.5S	90.8	Dawn	4171	2480	1198	1520	7	747
S12 Entry	2 Aug. 2005	7.1N	90.7	Dusk	810	2180	7571	1320	8	521
S12 Exit		2.7S	89.2	Dawn	615	2580	2018	1320		152
S13 Exit	20 Aug. 2005	0.5S	87.3	Dawn	865	3000	390	1780	23	35
S14 Entry	5 Sept. 2005	8.4S	93.3	Dusk	3091	1960	7733	1360	37	54

that finds, locks, and tracks the carrier of the Cassini signal and produces Doppler and ranging data as well as demodulates the telemetry. The other receiver, called the Radio Science Receiver (RSR), is an open loop receiver that is driven by a tuning predictions file generated by the Radio Science group on the basis of the latest navigation solution. The RSR is a digital receiver that has a set of bandwidths that can be chosen by the user. For a given bandwidth, a matching sampling rate produces complex samples that are delivered to the user at the completion of the station pass.

3. Data Processing and Analysis

[6] Digital samples of the in-phase and quadrature signal components were recorded at multiple sampling rates (and bandwidths) using the open loop Radio Science Receivers (RSR) of the DSN. Analysis results below are based on processing data recorded at 1 kHz bandwidth. The RSR as well as all subsystems of the Deep Space Network are driven by a highly stable frequency and timing system based on a hydrogen maser. Accurate antenna pointing is required especially at higher frequencies (e.g., Ka-band).

[7] The RSR data are processed by first detecting the signal carrier via software. A phase-locked loop or a series of Fast Fourier Transforms are typical detection methods depending on factors such as the signal-to-noise ratio as well as frequency and amplitude dynamics. Once detected, the signal is up-converted to "sky frequency" and then frequency residuals are produced by removing a model of the apparent relative motion between the spacecraft and ground station. These residuals contain the science information on the atmosphere/ionosphere of the planet, and form the basic data from which the atmospheric and ionospheric properties are extracted.

[8] The procedures for the analysis and inversion of these data are described in detail elsewhere [*Kliore et al.*, 2004]. The residuals are detrended by fitting a least-squares straight line to the baseline data and subtracting it from the raw residuals.

[9] The residuals are then used to compute the refractive bending angle at each data time point. This requires a precise ephemeris of Cassini relative to Saturn, iterative light propagation time solutions linking the spacecraft, Saturn, and the DSN station, and a representation of the local vertical direction at the measuring point in the Saturn ionosphere. This is given by the gravity field coefficients of Saturn (GM, J2, J4, and J6), and the rotation rate at the level in question. It provides one with the direction of the gravity vector, and the location of the instantaneous center of refraction is assumed to lie in that direction at a distance given by the radius of curvature of the equipotential surface along the direction of the radio ray [cf. *Lindal*, 1992]. Once the refractive bending angle and its corresponding ray asymptote distance with respect to the center of refraction are computed for each data point, the Abel integral transform [cf. *Kliore et al.*, 2004] is used to invert these data and to produce a vertical profile of refractivity.

[10] Since the radio refractivity is proportional to the electron density times the inverse square of the frequency, the electron density can be determined, as the frequencies are known very precisely.

[11] The altitude is determined by the location of the radio line of sight relative to the height of the 1-bar pressure

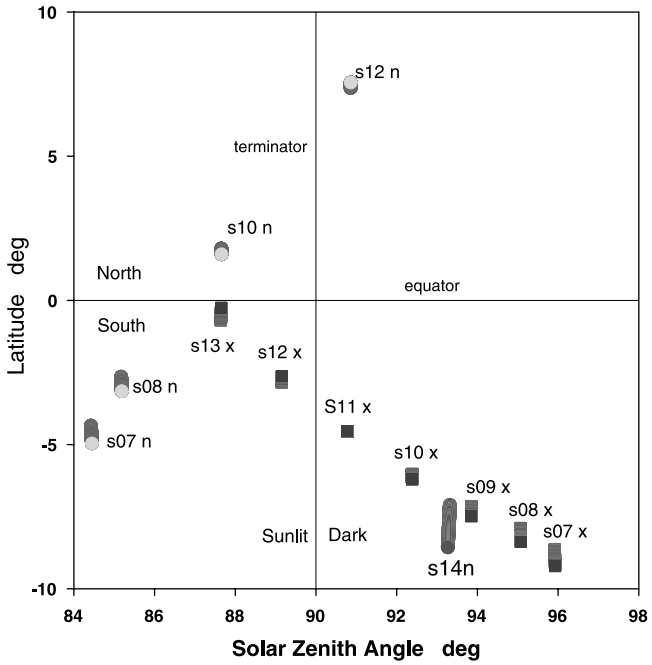

Figure 1. Latitudes and solar zenith angles of the first Cassini ionospheric radio occultations (x denotes exit and n denotes entry occultations).

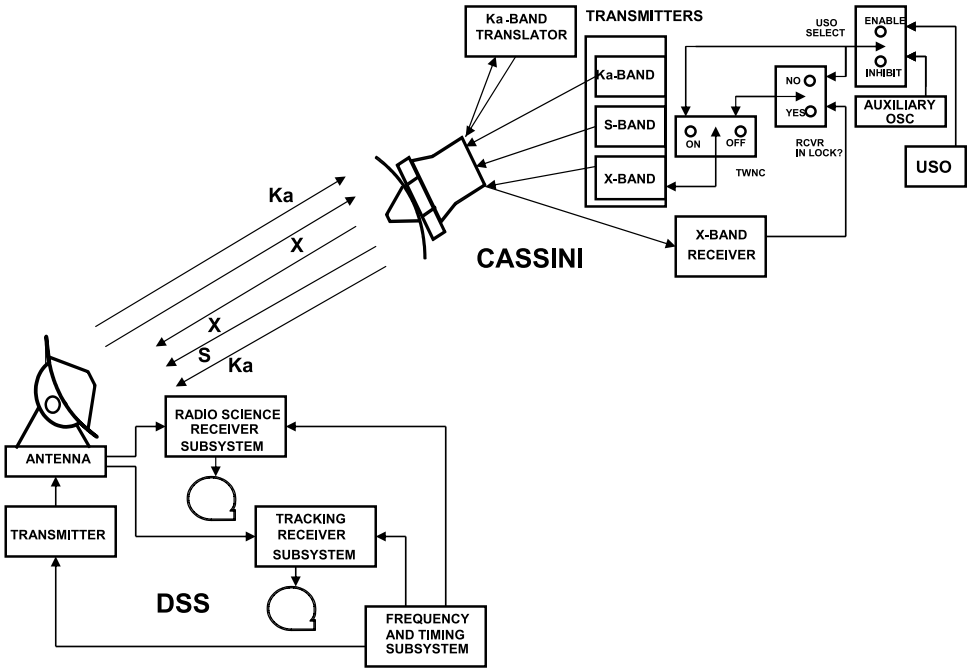

Figure 2. Schematic diagram of the Cassini radio science system, both on the spacecraft and on the ground.

surface at the latitude in question, the shape of which is calculated from the Saturn gravity field coefficients.

4. Results and Discussion

[12] The deduced electron density profiles obtained during the entry and exit occultations are shown in Figures 3 and 4, respectively. A number of general features are clearly identifiable. The peak densities are, in general, larger for the dusk results than for the dawn ones. However, it is useful to average all dusk and all dawn profiles for a clearer overall comparison; these are shown in Figure 5.

[13] The error bars in Figures 3 and 4 represent the uncertainties introduced by baseline frequency fluctuations (as they appear in the electron density profiles), and the effects of averaging of several data sets. The baseline fluctuations are caused mostly by plasma in the solar wind, which becomes more important as the radio line of sight approached closer to the Sun. This is apparent from the last two columns of Table 1, which lists the SEP (Sun-Earth-probe) angle for each observation, and the observed magnitude of the standard deviation of the baseline fluctuation. This is obtained by averaging the electron density points over a portion of the baseline (generally between 8000 and 9000 km) to obtain the baseline average, $\overline{n}_{e_{bj}}$. For the jth data set, the baseline sigma, σ_{bj}, which defines the standard deviation of the data, is then given by

$$\sigma_{bj} = \frac{\sqrt{\sum_i \left(n_{eij} - \overline{n}_{e_{bj}}\right)^2}}{\sqrt{B-1}}, \qquad (1)$$

where B is the number of baseline data points.

[14] Data for each observation are collected by multiple DSN stations, ranging from two to five, therefore data sets

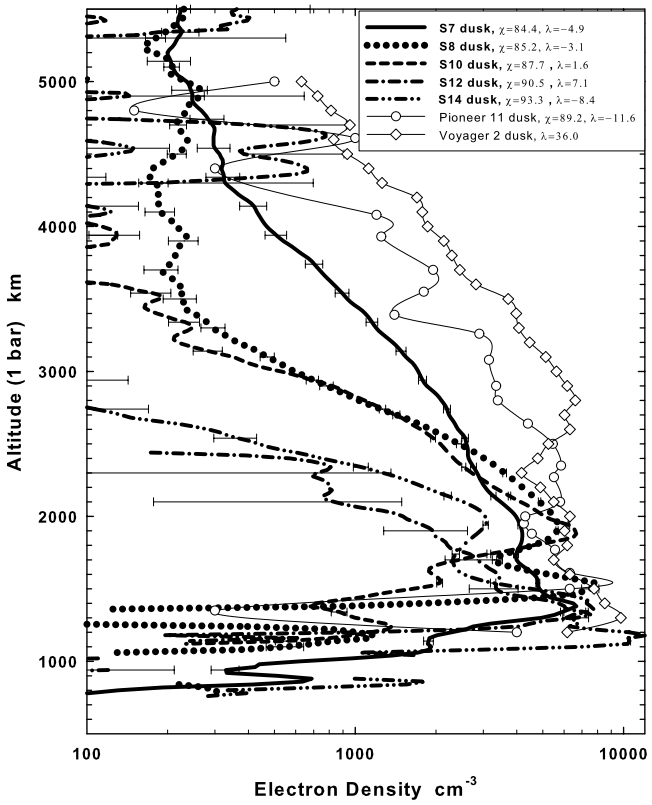

Figure 3. Observed entry (dusk terminator) electron density profiles. The Pioneer 11 [*Kliore et al.*, 1980] and Voyager 2 [*Lindal et al.*, 1985] dawn terminator observations are also shown for comparison.

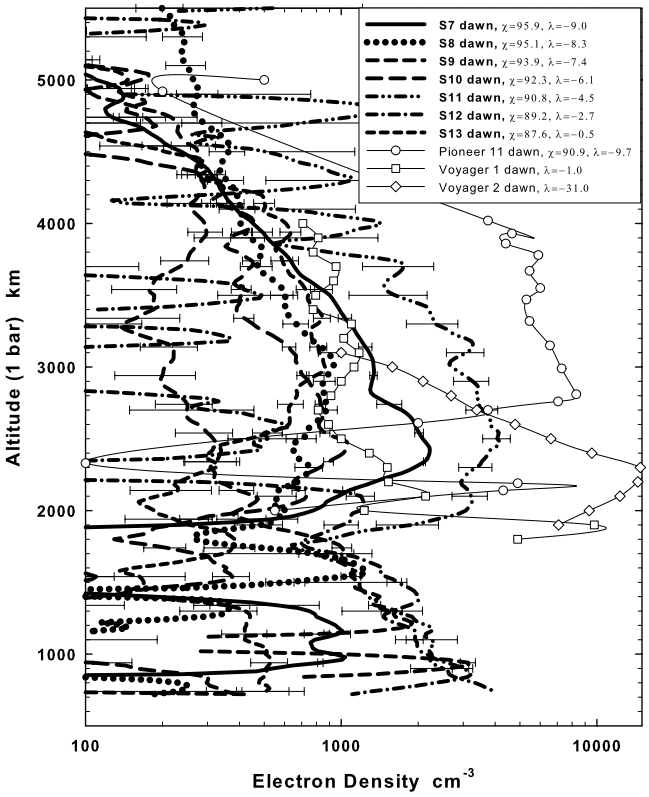

Figure 4. Observed exit (dawn terminator) electron density profiles. The Pioneer 11 [*Kliore et al.*, 1980] and Voyager 1 and 2 [*Lindal et al.*, 1985] dawn terminator observations are also shown for comparison.

must be averaged to obtain one electron density profile for each observation. So, if there are N data sets, the standard deviation of the average for each point i will be

$$\sigma_{A_i} = \frac{\sqrt{\sum_j \left(n_{e_{ij}} - \overline{n}_{e_i}\right)^2}}{\sqrt{(N-1)N}}, \tag{2}$$

where $\overline{n}_{e_i}$ is the average for point i from the N data sets. However, the baseline standard deviation must also be taken into account, and it propagates as

$$\sigma_{B_i} = \frac{1}{N}\sqrt{\sum_j \sigma_{bj}^2}, \tag{3}$$

and the total standard deviation for point i of the kth averaged observation is

$$\sigma_{ki} = \sqrt{\sigma_{A_i}^2 + \sigma_{B_i}^2}. \tag{4}$$

This is the quantity that is plotted as the error bars in Figures 3 and 4. which are obviously very different from one observation to another, reflecting the effect of the SEP angle, with the largest error bars occurring for those observations nearest to solar conjunction (Revs 11 and 12).

[15] When averaging the dusk and the dawn observations, it is desirable to weight the more accurate observations higher than the less accurate ones. For that purpose, a weighting factor is defined as follows:

$$w_{ki} = \frac{1}{\sigma_{ki}^2}. \tag{5}$$

It is convenient to normalize the weighting factors so that their sum is equal to the number of observations being averaged, K. Then, the normalized weighting factors become

$$w_{N_{ki}} = \frac{K w_{ki}}{\sum_k w_{ki}}. \tag{6}$$

The weighted average for point i is then

$$\bar{n}_{e_i} = \frac{1}{K}\sum_k w_{N_{ki}} n_{e_{ki}}, \tag{7}$$

and the standard deviation of the weighted average is

$$\sigma_{av_i} = \sqrt{\frac{\sum_k \left(\bar{n}_{ei} - w_{N_{ki}} n_{e_{ki}}\right)^2}{K(K-1)}}. \tag{8}$$

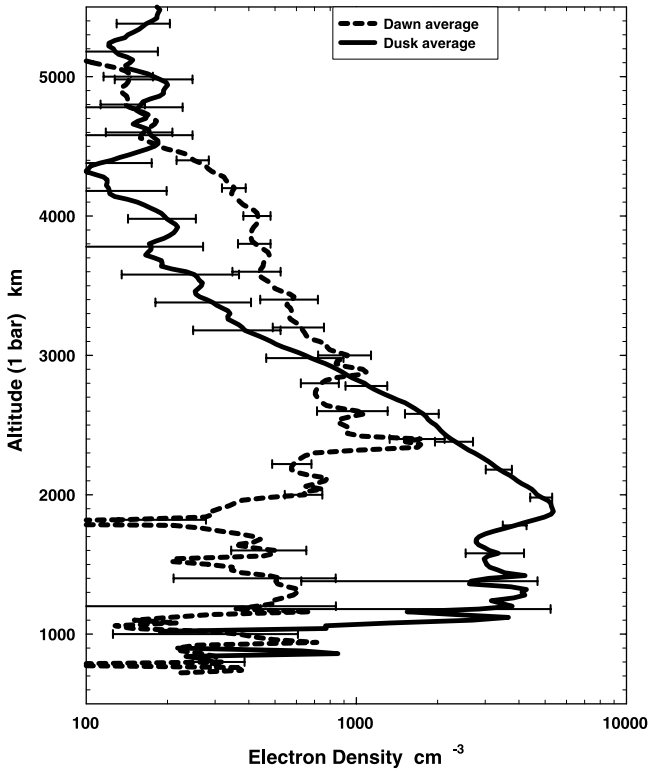

Figure 5. Weighted averages of dawn and dusk electron density profiles. When averaging, the data were weighted as the inverse square of the error bars shown in Figures 3 and 4.

The error standard deviation carried forward from each data set propagates to produce

$$\sigma_{p_i} = \frac{1}{K}\sqrt{\sum_k \left(w_{N_{ki}}\sigma_{ki}\right)^2}, \quad (9)$$

and finally, since the two errors described by equations (8) and (9) can be independent, the total one-sigma uncertainty of the weighted average is

$$\sigma_i = \sqrt{\sigma_{av_i}^2 + \sigma_{p_i}^2}. \quad (10)$$

This is the quantity that is plotted in the error bars on the averaged plots of Figure 5.

[16] The uncertainty in altitude is determined by the uncertainty in the projection of the position of the spacecraft relative to Saturn, which at the times of these measurements was less than 1 km (one-sigma).

[17] Clearly averaging removes some important features, such as differences in the altitude of the peak and topside scale height. These will be addressed later in this section. The mean main peak densities for the dusk and dawn conditions are about 5.4×10^3 cm^{-3} and 1.7×10^3 cm^{-3}, and the altitude of the peaks are at about 1880 km and 2360 km, respectively. The mean solar zenith angle for the dusk cases is approximately 95.1°, while it is 86° for the dawn observations. The Pioneer 11 and Voyager 1 and 2 egress measurements correspond to low latitudes and observed peak densities of about 1×10^4 cm^{-3}, values significantly larger than the mean values presented here. The Pioneer/Voyager observations were made during solar cycle maximum, while the Cassini data presented here come near minimum conditions. This cannot explain all the differences, but is likely the cause of some of them.

[18] There is no uniform agreement among the theoretical models regarding the major ion near the peak and on the topside. *Waite and Cravens* [1987] predict H_3^+ to be the major ion in these regions, but the more recent models of *Majeed and McConnell* [1996], *Moses and Bass* [2000] and *Moore et al.* [2004] suggest that H^+ is the main ion above the density peak. However, even these recent models indicate significant H_3^+ densities near and below the peak. The lifetime of these molecular ions is short, less then a few hundred seconds [*Moore et al.*, 2004], and thus significant decay is plausible during the approximately 5 hours of Saturn's nighttime. The mean observed decrease in the peak density and increase in the corresponding height are consistent with the presence of these molecular ions and the related decay. As the ionosphere decays at night, it is the bottomside which decreases more rapidly, where the loss rates are the largest, because of the higher neutral densities. Thus this preferential decrease below the peak will cause a decrease in the peak density and an increase in the altitude of the peak. Similar behavior is predicted and seen in the midlatitude terrestrial *F* region at night [cf. *Schunk and Nagy*, 2000].

[19] The observed relatively small dawn to dusk variation is contrary to the approximately two order of magnitude day to night differences implied by the Voyager 2 Saturn Electric Discharge (SED) observations [*Kaiser et al.*, 1984]. It needs to be noted that the noon to midnight variations are certainly expected to be greater than the dawn/dusk ones, but still the observed values presented here appear to be significantly less than the ratio implied by the Voyager observations. It also needs to be noted that very recently *Mendillo et al.* [2005] suggested that the interpretation of the SEDs in terms of peak electron densities may be wrong, because of ring shadowing effects.

[20] The next question one needs to address is the origin of the strong variability among the occultation results for the same local time conditions. All the results presented here come from a narrow range of latitudes, namely between about 10°S and 10°N. It is tempting to suggest that the differences must be caused by changes in the inflow of water from the rings. It was suggested some time ago that inflow of water from the rings play an important role in controlling the ionospheric densities [*Connerney and Waite*, 1984]; furthermore it has been proposed recently (H. Waite, personal communication, 2005) that the water comes into the ionosphere in the form of hydrated ions and thus follows magnetic field lines. Using the recent magnetic field model of Saturn (G. Giampieri, personal communication, 2005) the $-3°$ and $-10°$ latitudes map to equatorial distances of 1.0206 to 1.0673 R_s (Saturn radii), respectively. The smaller of these equatorial values correspond to an altitude of only about 1240 km, clearly a location well within the ionosphere. The larger value corresponds to about 4060 km and does correspond to the D-ring. The number of occultations is too small at this point to do any quantitative statistical study of the possible role of water on the variations, but we hope to look at this question later, as more data are obtained. Another possible reason for these variations may have to do with changes in particle impact ionization rates. At this time, the relative importance of photoionization versus impact ionization near the terminator is not clear. The Cassini CAPS results [e.g., *Young et al.*, 2005] do indicate that there are significant variations in the electron and ion number fluxes and their energies in the magnetosphere beyond about 3 R_s. Cassini has not and will not make any direct plasma observations in the close equatorial region corresponding to the ionospheric measurements reported here. However, it is not unreasonable to assume that there is also significant variability in the particle fluxes close to the planet, and thus the observed ionospheric variations may also, at least partially, be the result of changing particle fluxes.

[21] Finally, we look at the topside scale heights of the observed electron densities. It is certainly very risky to interpret vertical plasma scale heights so near the equator (mean dip angle of about 13°). Nevertheless that is all we have available at this time, and we will probably not have any more definitive information concerning Saturn's equatorial ionosphere for decades. Therefore we proceed and see what we can infer by assuming that the profiles shown in Figure 5, correspond to diffusive equilibrium conditions, but at the same time we must be highly "skeptical" of the results. In Saturn's ionosphere the altitude where the transition from chemical to transport control takes place is generally believed to be somewhere below the ionization peak, although *Moore et al.* [2004] suggest that this transition may be as high as 2500 km. If we now assume that the topside results above 2500 km correspond to diffusive equilibrium conditions, the sim-

plified momentum equation can be written in terms of the plasma density gradient as

$$\frac{1}{n_e}\frac{\partial n_e}{\partial r} = -\frac{1}{H_p} - \frac{1}{T_p}\frac{\partial T_p}{\partial r}, \quad (11)$$

where the plasma scale height, H_p, is

$$H_p = \frac{(T_e + T_i)}{m_i g}. \quad (12)$$

It is common to use the topside scale height to estimate the plasma temperature. However, not having direct information on either the ion composition or the temperature gradients, even with the assumption of diffusive equilibrium conditions, one must be aware of further limitations/shortcomings of this approach.

[22] The mean, observed topside scale heights for the dusk and dawn occultations are about 500 km and 1230 km, respectively. If one neglects temperature gradients, the uncertainty in the ion composition can lead to further large uncertainties in the corresponding plasma temperature. As mentioned earlier, there is no consensus among the available models regarding the major ion on the topside. However, it is not unreasonable to accept and use H^+ as the major topside ion for the dawn conditions and to further neglect temperature gradients. With these assumptions, the observed topside dawn scale heights imply a plasma temperature of about 625°K. Next, if we accept that the dusk temperature should be at least as large as the dawn one, we arrive at a mean ion mass of about 2.46 amu. This could imply the presence of about 72% H_3^+ or about 7.7% of H_3O^+ or some appropriate combination of these ions being present. Furthermore, we neglected any temperature gradients in arriving at these results, but as an example, if the true plasma temperature is 1000°K, a small temperature gradient of only about 1.6°K km^{-1} could lead to the observed dusk plasma scale height. This is not an unreasonably large gradient; even larger temperature gradients were predicted for the ionosphere of Saturn by the model of *Frey* [1997] and for the ionosphere of Jupiter by the model of *Nagy et al.* [1976].

5. Summary

[23] In this paper we have presented the first set of ionospheric radio occultation results obtained by the Cassini spacecraft in the May to September period in 2005. A total of twelve occultations were obtained, which is about double of those obtained by the Pioneer and Voyager spacecraft. This increased database, although limited to equatorial latitudes, does provide further insights into the nature of Saturn's ionosphere. However, we still have too many unknown and unrestrained parameters (e.g., plasma temperatures and ion composition) to be able to arrive at a definitive understanding of the physical and chemical processes controlling the ionosphere, but the results presented here do provide an envelope, described and discussed in this paper, within which the true answers must lie. We will obtain numerous more electron density profiles, covering different latitudes and solar conditions, during the lifetime of the Cassini mission, which will add to our knowledge base and help to advance our understanding of Saturn's ionosphere, but we will have to wait for another mission which can directly measure the "missing" parameters, before we can say with confidence that we fully understand the ionosphere of Saturn.

[24] **Acknowledgments.** The work described in this paper was supported by the Cassini Program at JPL. One of the authors, A.F.N., was also partially supported in this work by NASA grant NAG5-13332.

[25] Arthur Richmond thanks Ingo Mueller-Wodarg and Luke Moore for their assistance in evaluating this paper.

References

Connerney, J. E. P., and J. H. Waite (1984), New model of Saturn's ionosphere with an influx of water from the rings, *Nature*, *312*, 136.

Frey, M. A. (1997), The polar wind of Saturn, Ph. D. thesis, Univ. of Mich., Ann Arbor.

Kaiser, M. L., M. D. Desch, and J. E. P. Connerney (1984), Saturn's ionosphere: Inferred electron densities, *J. Geophys. Res.*, *89*, 2371.

Kliore, A. J., I. R. Patel, G. F. Lindal, D. N. Sweetnam, H. B. Hotz, J. H. Waite Jr., and T. R. McDonough (1980), Structure of the ionosphere and atmosphere of Saturn from Pioneer 11 Saturn radio occultation, *J. Geophys. Res.*, *85*, 5857.

Kliore, A. J., et al. (2004), Cassini radio science, *Space Sci. Rev.*, *115*, 1.

Lindal, G. F. (1992), The atmosphere of Neptune: An analysis of radio occultation data acquired with Voyager 2, *Astron. J.*, *103*(3), 967.

Lindal, G. F., D. N. Sweetnam, and V. R. Eshleman (1985), The atmosphere of Saturn: An analysis of the Voyager radio occultation measurements, *Astron. J.*, *90*, 1139.

Majeed, T., and J. C. McConnell (1996), Voyager electron density measurements on Saturn: Analysis with a time dependent ionospheric model, *J. Geophys. Res.*, *101*, 7589.

Mendillo, M., L. Moore, J. Clarke, I. Mueller-Wodarg, W. S. Kurth, and M. L. Kaiser (2005), Effects of ring shadowing on the detection of electrostatic discharges at Saturn, *Geophys. Res. Lett.*, *32*, L05106, doi:10.1029/2004GL021175.

Moore, L. E., M. Mendillo, I. C. F. Müller-Wodarg, and D. L. Murr (2004), Modeling of global variations and ring shadowing in Saturn's ionosphere, *Icarus*, *172*, 503, doi:10.1016/j.icarus.2004.07.007.

Moses, J. I., and S. F. Bass (2000), The effects of external material on the chemistry and structure of Saturn's ionosphere, *J. Geophys. Res.*, *105*, 7013.

Nagy, A. F., W. L. Chameides, R. H. Chen, and S. K. Atreya (1976), Electron temperatures in the Jovian ionosphere, *J. Geophys. Res.*, *81*, 5567.

Schunk, R. W., and A. F. Nagy (2000), *Ionospheres*, Cambridge Univ. Press, New York.

Waite, H. W., and T. E. Cravens (1987), Current review of the Jupiter, Saturn and Uranus ionospheres, *Adv. Space. Sci.*, *7*(12), 119.

Young, D. T., et al. (2005), Composition and dynamics of plasma in Saturn's magnetosphere, *Science*, *307*, 1262.

A. Anabtawi, S. W. Asmar, E. Barbinis, D. Fleischman, G. Goltz, D. Johnston, A. J. Kliore, and N. J. Rappaport, Jet Propulsion Laboratory, California Institute of Technology, Pasadena, CA 91109, USA.

M. Flasar, NASA Goddard Space Flight Center, Greenbelt, MD 20771, USA.

R. French, Astronomy Department, Wellesley College, Wellesley, MA 02481, USA.

E. Marouf, Department of Electrical Engineering, San Jose State University, San Jose, CA 95192, USA.

A. F. Nagy, Department of Atmospheric, Oceanic, and Space Sciences, University of Michigan, Ann Arbor, MI 48109, USA. (anagy@umich.edu)